IOP Publishing | International Atomic Energy Agency Nuclear Fusion

Nucl. Fusion **56** (2016) 112016 (9pp) doi:10.1088/0029-5515/56/11/112016

Multiple toroidal Alfven eigenmodes with a single toroidal mode number in KSTAR plasmas

H. Rizvi[1], C.M. Ryu[1] and Z. Lin[2]

[1] Department of Physics, POSTECH, Pohang, Korea
[2] Department of Physics and Astronomy, University of California Irvine, CA 92697, USA

E-mail: ryu201@postech.ac.kr

Received 4 January 2016, revised 22 May 2016
Accepted for publication 7 June 2016
Published 28 July 2016

Abstract

Simultaneous excitation of multiple discrete toroidal Alfven eigenmodes (TAEs) for a single toroidal mode number have been observed in KSTAR plasmas. Excitation and characteristics of these modes are studied by using a global gyrokinetic particle-in-cell simulation code. It is shown that compared to a single core-localized mode, excitation of two modes is difficult. The frequency difference between the double TAEs studied from simulation seems to agree well with the experimental value. Details of studies on the frequency, growth rate, mode structures, etc, using the GTC simulation are presented.

Keywords: TAE, Alfven eigen mode, gyrokinetic simulation, particle-in-cell simulation, KSTAR, GTC

(Some figures may appear in colour only in the online journal)

1. Introduction

There has been much interest in Alfvenic waves driven by energetic particles because of their potential importance in fusion grade burning plasmas [1, 2]. In toroidal plasmas, Alfvenic modes, which are weakly damped eigenmodes, can be easily destabilized by energetic ions and can degrade the fast ion confinement. Toroidal Alfven eigenmodes (TAEs) and reversed shear Alfven eigenmodes (RSAE) are such modes that are driven unstable by energetic ions in toroidal plasmas, which are currently actively studied [3, 4]. TAEs have been observed in many different tokamaks [5–9], and understanding the various properties of TAEs is important for the burning plasma like the ITER plasma [10, 11].

In ITER, one of the main loss mechanisms for fast ions is expected to be the enhanced transport caused by multiple TAE excitation [10]. This is part of the reason for the recent interest in multiple modes [12] and their effects on particle transport [13–18]. For instance, Schneller *et al* [16] in a recent work modeled fast particle transport driven by multi n-mode Alfvenic activity, by using the HAGIS code for the nonlinear simulation, and comparison with the ASDEX Upgrade experiment [19]. They observed that the phase space channeling effect caused by the presence of multiple modes can enhance the losses in the orders of magnitude. Another effect of multiple mode coupling is the flattening of the spatial profiles due to enhanced fast ion transport. White *et al* [14] observed in guiding center simulation that once the multiple TAE activity develops these modes can produce a substantial central flattening of the beam distribution. Multiple TAE modes with different toroidal mode numbers (n) are observed and have been studied in DIII-D [20] and in other toroidal plasmas like JET [4], NSTX [21], and TJ-II [22].

In 2014 KSTAR [23] experiments, we have observed multiple TAEs at frequencies in the range of 142–175 KHz in Mirnov coil (MC) diagnostics, where the shots have maximum plasma currents $I_p = 700$ kA, magnetic fields $B = 2$–3 T and with three NBI with energies 80, 80 and 95 KeV, which induced fast particles at velocities 2.7×10^8 cm s^{-1} and 2.9×10^8 cm s^{-1}, respectively. For the typical range of electron densities 2.8–0.9×10^{13} cm^{-3} in KSTAR, the Alfven velocities are of the order of 1.58×10^8 cm s^{-1}–1.54×10^9 cm s^{-1}, respectively. The mode analysis shows that some of these modes appear as a pair to have the same toroidal mode number

$n = 2$. Multiple TAEs are commonly observed in tokamaks [4, 19, 20], but the dual modes with a single n number observed in KSTAR seems somewhat special. We suspect that the occurrence of such dual modes might have been associated with the injection characteristics of neutral beams in KSTAR, especially in the case of off-axis heating. During the initial phase of the NBI injection, the fast particle density profiles of the NBI driven plasmas could vary unevenly. We, thus, have investigated the effect of the non-uniform density profile on the excitation of multiple TAEs with a single n by using the gyrokinetic toroidal code (GTC) [24–26], and found that two localized modes at different radial positions can be excited simultaneously, but that the second mode located outside is more difficult to excite than the first core-localized mode. This seems to explain why TAEs appear normally as a single mode for a given toroidal number in KSTAR. In the literature, most of the simulation works on TAEs have focused on the excitation and characteristics of a single mode for a given toroidal number [27–35].

In this work, we report an observation of dual TAEs in KSTAR plasmas during the early phase of neutral beam injection and their possible excitation by using a simulation study. This manuscript is organized in the following manner. In section 2, the observation of multiple TAEs in KSTAR experiments is presented. The mathematical model of the localized TAEs is described in section 3. In section 4 we present the conditions for our gyrokinetic particle-in-cell simulation. In section 5, the results and discussions are given with comparison to experimental observations. Section 6 is given for the conclusion of this study.

2. Experimental observation

In KSTAR, extensive experiments have been performed in order to detect the toroidal Alfven eigenmodes (TAEs) with a heating power of up to 5 MW. In these experiments, deuterons with energies of up to 90 and 80 KeVs are injected by using a neutral beam heating system, which consists of three NBIs. These NBI passing energetic particles with the parallel velocity $v_{\|} = v_A/3$ could resonate with shear Alfven waves in typical KSTAR plasmas with ($B = 2.687$ T, $n_e = 2 \times 10^{13}$ cm^{-3}). Alfvenic activities were clearly observed in the L-mode plasma discharge (#10574) performed in KSTAR, where $R = 180$ cm, $a/R = 0.227$, $I_p = 0.7$ MA, $B_t = 2.688$ T, with all three NBIs are used. In addition to the NBI heating the electron cyclotron current drive (ECCD) is used at a very early time (before the NB injection) to preheat the plasma electrons up to temperature 4–10 KeVs. 2nd harmonic ECCD is used with power 0.75 MW. The expected heating location is $R_{res} \simeq 142$ m. Heating and current conditions are shown in figure 1(a), the spectrogram of NBI driven Alfvenic activities are presented in figure 1(b) and corresponding mode number analysis is given in figure 1(c). The NBIs are injected with the time delay of 500 ms which induced ladder-like multiple Alfven activities. In the experiment, the sampling rate of MC diagnostic is 500 KHz, which is enough for the measurement of the TAE activity in KSTAR. In typical KSTAR experiments, the rotation frequency is less than 10 KHz, the thermal ion transit frequency is about 30 KHz. The fishbone activity is normally below 20 KHz, the EPM usually appears near 100–120 KHz, and the TAEs appear in the range of 130–200 KHz. The principal diagnostics currently available for the observation of TAE modes are magnetic diagnostics, which consists of a poloidal array of 22 MCs and a toroidal array of 20 MCs. ECE arrays and soft x-ray detectors are used as supplementary. An ECE array and soft x-rays are good detectors to cross check the TAEs, but for the KSTAR plasma discharge being investigated are set at low sampling rates of less than 100 kHz, and are not useful at the moment. KSTAR does not have enough computing capabilities yet to store high frequency sampling data of all the signals. The data from the 14 working toroidal MC channels are used for the toroidal mode number analysis. Our mode analysis shows (figure 1(c)) that different discrete modes inside the TAE frequency gap with the same toroidal mode number during the time of the second and third neutral beams are injected consecutively. Similar observations of the multiple modes in TAE gap are observed in several other KSTAR plasma discharges.

Simulation results for the fast particle distribution of the NBI heating are given in figure 2, from the super-code NTCC module NBEAM [36], based on the diffuse-beam model [37]. Using the plasma parameters of the above plasma discharge at $t = 1658$ ms and using the KSTAR NBI system specifications. For the cases of co-moving three deuterium NBIs with energy energies 90, 80 and 80 KeV, the center lines of the beams injected are at 148.6, 172.0 and 124.5 cm, respectively. All the beams have 'rectangular' shapes and 'rectangular' beam apertures of the beam half-width $\sigma_R = 22.5$ cm and the beam half-height $\sigma_Z = 60$ cm. The fraction of power in the full and half energy component for all beam lines is 0.75 and 0.2, respectively. The numerically estimated profiles of the total driven current, power deposition and fast particle density profiles are shown in figure 2 (black curves). Grey lines in figure 2 correspond to the case when the size of the beam is reduced to half i.e. $\sigma_R/2$ and $\sigma_Z/2$, with other NBI parameters fixed. Nonuniform radial variation in the profile is shown. This kind of nonuniformity, which depends on the beam geometry, is a typicial characteristic of the NBI driven heating and current drive as reported in [38]. In our NBEAM simulation, the effects of ramp-up current and off-axis ECCD preheating are ignored.

During the initial phase of the NBI injection in KSTAR, the fast particle density profiles of the NBI driven plasmas vary unevenly. Figure 2 of numerical simulation results for the NBI heating shows a nonuniform density profile. Thus, the occurrence of multiple modes with a single n in KSTAR might be associated with the injection characteristics of neutral beams in KSTAR, such as the off-axis heating.

3. Mathematical model

In this section, the mathematical model used in our linear GTC simulation is described. In simulations we follow the GTC electromagnetic formulation in which both ions, thermal

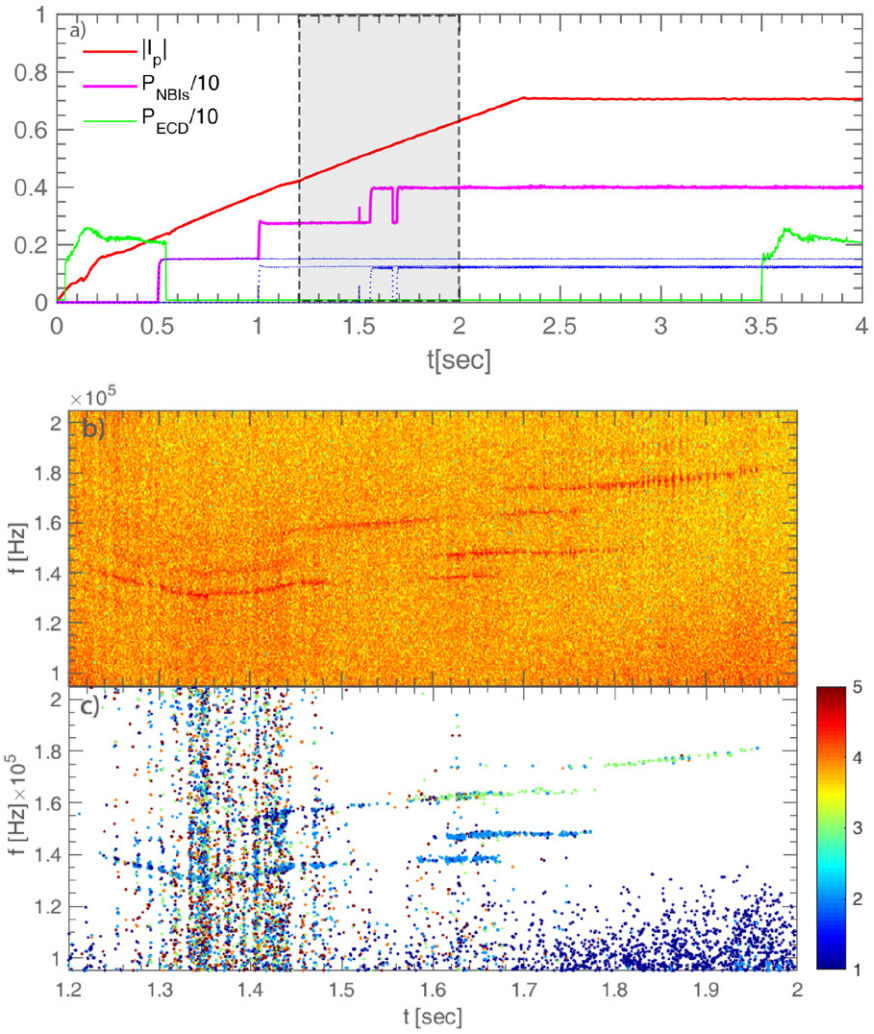

Figure 1. (*a*) Plasma current (in MA) and heating (in MW) conditions of KSTAR plasma discharge #10574 (blue) power of each NBI in units of (MW/10), (*b*) frequency spectrogram of the Mirnov data showing the multiple TAEs, and (*c*) corresponding mode number analysis.

and fast, are described by the gyrokinetic equation. The gyrokinetic model in the 5D phase space (gyrocenter position $\mathbf{X}$, magnetic moment μ, and parallel velocity $v_\parallel$) consists of the following equations [26, 39],

$$(\partial/\partial t + (v_\parallel \mathbf{B}/B_0)\cdot\nabla + \mathbf{v}_{*\alpha}\cdot\nabla + \dot{v}_\parallel\partial_\parallel) f_\alpha(\mathbf{X},\mu,v_\parallel,t) = 0, \tag{1}$$

$$\dot{v}_\parallel = -(Z_\alpha/m_\alpha c)\partial\delta A_\parallel/\partial t - (1/m_\alpha B_0)(\mathbf{B}_0^* + \delta\mathbf{B})\cdot(\mu\nabla B_0 + Z_\alpha\nabla\delta\varphi), \tag{2}$$

$$\delta\mathbf{B} = \nabla\times(\delta A_\parallel \mathbf{b}_0), \tag{3}$$

where m_α and Z_α are the mass and charge of the α-species, index $\alpha = e, i$ and f stands for the particle species (electron, ion and fast particle). $\mathbf{v}_{*\alpha} = \mathbf{v}_E + \mathbf{v}_c + \mathbf{v}_g$, $\mathbf{v}_E = (c\mathbf{b}_0\times\nabla\delta\varphi)/B_0$, $\mathbf{v}_c = (v_\parallel^2/\Omega_\alpha)\nabla\times\mathbf{b}_0$ and $\mathbf{v}_g = (\mu/m_\alpha\Omega_\alpha)(\mathbf{b}_0\times\nabla B_0)$ being the $\mathbf{E}\times\mathbf{B}$, curvature and grad-$B$ drifts, respectively. $\delta\varphi$ is the gyroaveraged electrostatic perturbation and $A_\parallel$ is the gyroaveraged vector potential. $\mathbf{B} = \mathbf{B_0} + \delta\mathbf{B}$ with the equilibrium magneticfield is $\mathbf{B} = B_0\mathbf{b_0}$ and $\mathbf{B_0^*} = (B_0 v_\parallel/\Omega_a)\nabla\times\mathbf{b}_0$. In the GTC, electrons follow the kinetic hybrid electron model [26], in which electrons are treated adiabatically in the zeroth order and kinetically in the higher order. In our simulation we have assumed electrons to be adiabatic and the electron continuity equation is the same as equation (28) of [40] except the last four nonlinear terms. In the ideal MHD limit, the fluid continuity equation can be retrieved by taking the moment of equation (1) in the lowest order and by ignoring the plasma current, we have

$$\begin{aligned}&\partial\delta n_e/\partial t + \mathbf{B_0}\cdot\nabla((n_{e0}\delta v_{e\parallel})/B_0) + B_0\mathbf{v_E}\cdot\nabla(n_{e0}/B_0)\\ &\quad - (1/m_e\Omega_e)(\mathbf{b_0}\times\nabla(\delta P_{e\parallel} + \delta P_{e\perp})\cdot(\nabla B_0/B_0))\\ &\quad - n_{e0}\mathbf{v_E}\cdot(\nabla B_0/B_0) = 0.\end{aligned} \tag{4}$$

This equation is the same as equation (10) in [26]. In the zeroth order $\delta P_{e\parallel}^{(0)} = \delta P_{e\perp}^{(0)} = n_{e0} e\delta\varphi_{\rm eff}$, where $\delta\varphi_{\rm eff}$ is the effective potential which represents the perturbed parallel electric field in such a manner that $\delta E_\parallel = -\mathbf{b_0}\cdot\nabla\delta\varphi_{\rm eff} = \mathbf{b}_0\cdot\nabla\delta\varphi - (1/c)\partial A_\parallel/\partial t$. The remaining two equations in the model are gyrokinetic Poisson's equation and the inverse parallel Ampere's law,

$$(Z_i^2 n_i/T_i)(\delta\varphi - \delta\tilde{\varphi}) = \sum_{\alpha=e,i,f} Z_\alpha\delta n_\alpha, \tag{5}$$

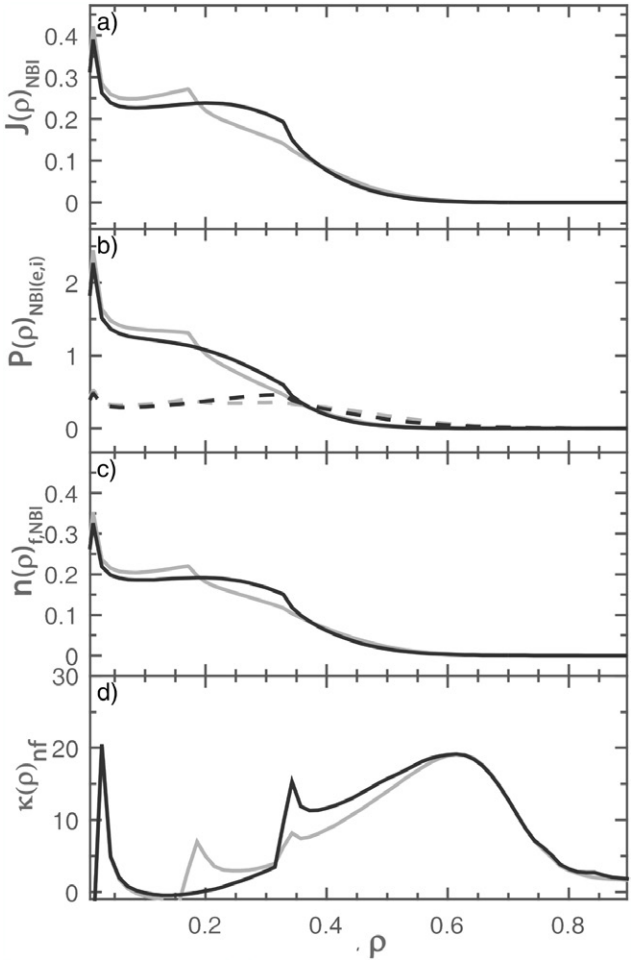

Figure 2. Numerical simulation results of NBEAM for the NBI heating; (*a*) total neutral beam driven current density in A m^{-2}, (*b*) beam heating power to ions (solid) and electrons (dashed) in MW m^{-3}, (*c*) NBI fast ion density in 10^{19} m^{-3} and (*d*) profile of NBI fast ion density gradient κ_{nf}.

and

$$4\pi e\delta v_{e\|} = 4\pi(Z_i\delta v_{i\|} + Z_f\delta v_{f\|}) - c\nabla_\perp^2\delta A_\|, \tag{6}$$

respectively, where $\delta\bar{\varphi}$ is the gyro averaged potential. Considering $E_\| = 0$, and retaining only the linear terms, our mathematical model equation in the long wave length limit reduces to

$$\omega^2\nabla_\perp\cdot(\nabla_\perp\delta\varphi)/v_A^2 = -\mathbf{B_0}\cdot\nabla\left[(1/B_0)\nabla^2(b_0\cdot\nabla\delta\varphi)\right], \tag{7}$$

which is the eigenmode equation for the shear Alfven wave. Using the Fourier transform $\delta\varphi(r,\theta,\zeta,t) = \sum_m \delta\varphi_m(r)\exp(-im\theta + in\zeta - i\omega t)$ and $B \approx B_0(1 - r\cos\theta/R)$, one can find the two poloidal harmonics $\delta\varphi_m$ and $\delta\varphi_{m+1}$ coupled at the center of two rational surfaces to create a toroidicity induced gap in the Alfven continuum at frequency

$$\omega^2(r) = v_A^2(r)k_\|^2 = v_A^2(r)/4q^2(r)R^2, \tag{8}$$

where $q(r)$ is the safety factor at the mode radial location, i.e. at r_m or r_{m+1}. Value of the safety factor at r_m is $q(r_m) = (m - 1/2)/n$. In our simulation we have considered the excitation of two linear modes at radial locations $r_{m-1,\,m}$ and $r_{m,\,m+1}$. The dispersion relation in equation (8) is locally valid. For a single TAE the radial width can be estimated as [41],

$$\delta_m = \begin{cases} (r_m/m)\sqrt{\varepsilon/s} & s \ll \varepsilon \\ (r_m/m) & s \lesssim 1 \end{cases} \tag{9}$$

Here, $\varepsilon = (5/2)(r/R_0)$ and s is the magnetic shear defined as

$$s = (r/q)(\mathrm{d}q/\mathrm{d}r). \tag{10}$$

δ_m is an important parameter which decides the type of TAE to be localized or global [42], depending upon the plasma shear, the poloidal mode number and the mode location. Qualitatively the higher the s and/or m, the mode will have a smaller radial width. The modes localized away from the core may have larger radial widths compared to the core-localized mode, depending upon m and s. The distance between the two neighboring TAE gaps can be estimated from $q(r_m) = (m - 1/2)/n$ as $\Delta r = r_m/(s(m - 1/2))$, and, thus, when $\delta_m > \Delta r/2$ overlapping between the neighboring poloidal harmonic occurs, which will then excite a global type TAE mode. Combining both length scales, one can find the critical shear as,

$$s_c = m^2/(4\varepsilon q^2 n^2), \tag{11}$$

for case of $s \ll \varepsilon$, and for case of $s \lesssim 1$

$$s_c = m/(2qn). \tag{12}$$

This gives a value of critical shear s_c below which discrete TAEs will appear and for $s > s_c$ global type TAE will appear. For the KSTAR experiment, the value of the critical shear turns out to be $s_c \simeq 1.309$ and $s(r/a) < s_c$ for $r/a < 0.75$, and thus in the first two TAE gaps the mode will have discreate/localized structure. By assuming the mode to be excited at the center of the gap and ignoring the radial variation of v_A, i.e. $v_A(r_m) \approx v_A(r_{m+1})$, a simple theoretical estimation for the frequency difference between the component of multiples TAE can be obtained as,

$$\Delta\omega \simeq nv_A/(2R(m^2 - 1)), \tag{13}$$

or by using $\Delta r = r_m/(s(m - 1/2))$, in a more practical form as,

$$\Delta\omega \simeq (v_A/2R)(s\Delta r/r_m q_{m+1}), \tag{14}$$

where $q_{m+1} = q(r_{m+1})$. From equation (13), the higher the n, the larger will be the frequency difference between the two TAEs.

4. Simulation setup

The fast particle profile shown in figure 2 indicates that the density gradient can change sharply with a small change of nonuniformity with several peaks of the gradient values, but this profile cannot still be taken as fully representing the real situation, because some important physics mechanisms such as the ramp-up current, nonuniform local transport, nonlinear wave-particle interaction, etc are not included. Since our main interest is a dual TAEs with a single n and their

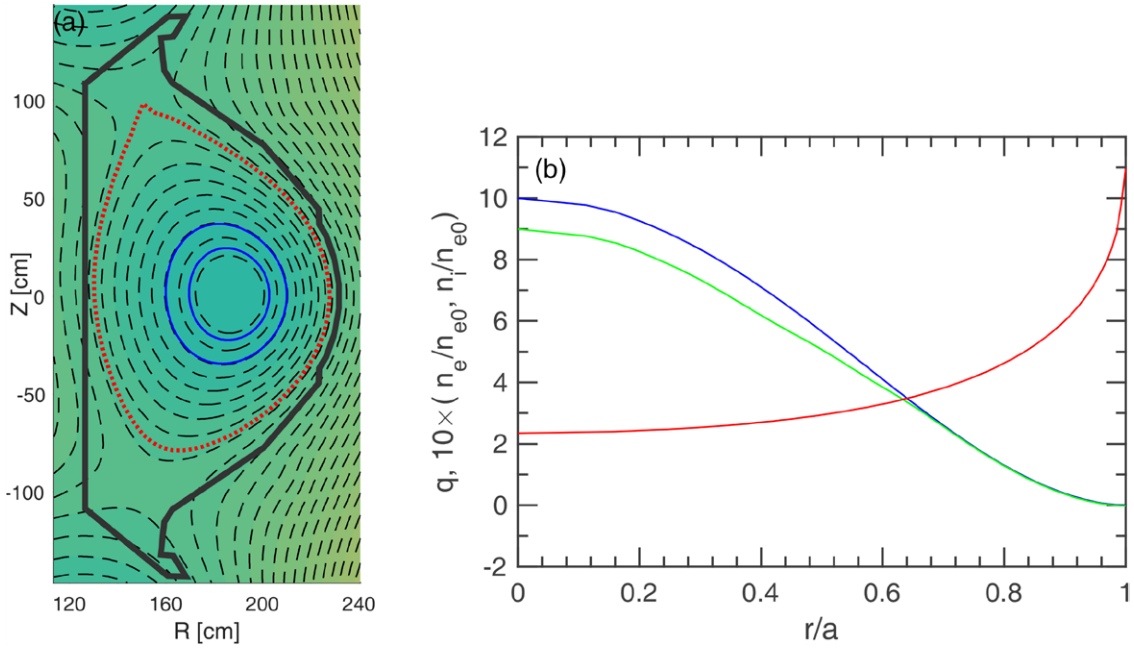

Figure 3. (*a*) Magnetic flux surfaces, where the red line shows the last closed flux surface. (*b*) Electron (blue line), ion (green) densities, and q(red) profile.

characteristics, to simplify the problem, we instead have considered an analytical profile (given by equation (15)) with a double peak density gradient and focused on investigating its gradient effect.

$$n_f/n_{f0} = n_c + n_1 \tan h[(n_3 - \tilde{\psi})/n_4] + n_2 \tan h[(n_5 - \tilde{\psi})/n_6] \tag{15}$$

where $n_c = 1 - (n_1 + n_2)$, n_i (with $i = 1$–6) are profile parameters and $\tilde{\psi}$ is the normalized flux function. We have considered a KSTAR equilibrium of plasma discharge #10574 at $t = 1658$ ms as the case study, which has a D-shape cross-section with the elongation $\kappa = 1.8$ and the triangularity $\delta = 0.55$. To refine plasma profiles and magnetic geometry data from the EFIT, the CHEASE code is used to reconstruct the equilibrium [43]. In the simulation, the background plasma density, temperature profiles, flux surface structure, the field magnitude, and the q-profile are taken from the reconstructed CHEASE equilibrium and are used in a recent version of the GTC with realistic geometry implemented [44]. Fast particles are included using the quasi-neutrality $\sum_\alpha Z_\alpha n_{\alpha 0} = 0$ where Z_α is the effective charge and $\alpha = e, i, f$, and hence, the quasi-neutrality is maintained in the zeroth order in the simulation. The plasma equilibrium has a magnetic field on the axis $B_0 = 2.688$ T, and the safety factor at the axis is $q_0 = 2.345$. The discharge is characterized by a relatively low sheared q-profile. The on-axis electron density is $n_{e0} = 2.4 \times 10^{13}\,\mathrm{cm}^{-3}$ and the ion and electron temperatures are $T_{i0} = T_{e0} \simeq 4$ keV (these parameters correspond to a bulk plasma with $\beta_e \simeq 0.5\%$). The initial densities and q profiles are as shown in figure 3. The plasma consists of deuterium ions and electrons. The unperturbed velocity distribution functions are assumed to be shifted Maxwellian with a thermal velocity $v_{th\alpha} = \sqrt{T_{\alpha 0}/m_\alpha}$ given by [26],

$$f_{\alpha 0} = n_{\alpha 0}/(2\pi T_{\alpha 0}/m_\alpha)^{3/2} \exp[-(\mu B_0/ + m(v_\parallel - u_{\parallel 0})^2/2)/T_{\alpha 0}], \tag{16}$$

where $u_{\parallel 0}$ is the equilibrium parallel flow velocity, with the fast particle temprature $T_f \simeq 40 T_e$. In comparison, the anisotropic NBI distribution function with finite pitch angle dependance and the same pressure gradient profile, in general, affect the moderate n TAEs [45] directly by the additional velocity space drive and indirectly by increasing the density of resonant fast particles [46]. Moreover with an isotropic distribution function both trapped and passing particles contribute in resonance, whereas only passing particles contribute in resonance due to strong pitch angle dependance in distribution. In this work both the ion and fast particles are treated gyrokinetically in the GTC code, whereas electrons are taken to be adiabatic. We have considered a perfectly conducting wall as a boundary condition. In all simulations presented here, computational grids consist of 32 grids in the parallel direction and 64 grids in the radial direction. The number of poloidal grids are 38 in the innermost surface and 128 in the outer most surface, and therefore, the total number of grids on a poloidal plane is 8385. The time step is $\Delta t \approx 0.1 R/v_{\mathrm{A}0}$, where $v_{\mathrm{A}0}$ is the Alfven velocity at the central axis in the toroidal direction. Other plasma parameters are $k_\theta \rho_f \simeq 0.51$, $k_\theta \rho_i \simeq 0.12$, and $\beta_f \simeq 0.06$, where k_θ is the poloidal wave number, ρ_i and ρ_f are the ions and fast ions gyroradius, respectively.

Our study was limited only to the linear simulation for a single toroidal mode number, $n = 2$ (selected from the mode number analysis of KSTAR discharge #10574), with no restriction on the poloidal harmonics. The diamagnetic drift velocity of fast particles can provide a free energy to excite TAE, and thus the growth rate can vary with beta and diamagnetic drift frequency of the fast ions. Thus, $\kappa_{\mathrm{nf}} \equiv -(R/n_f)(\partial n_f/\partial r)$, which is the profile of the fast ion density gradient, becomes

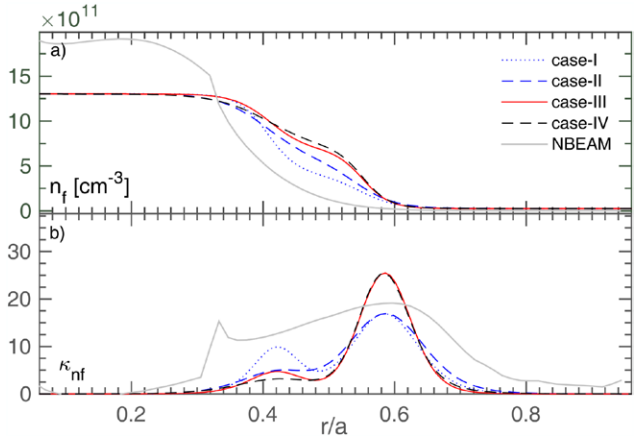

Figure 4. (*a*) Fast particle density profiles, and (*b*) corresponding fast particle density gradient profiles, for all the cases, along with the NBEAM approximation (grey).

a control parameter in our study. In a conventional case $\kappa_{nf}(r)$ peaked at the mode rational surface, where the two consecutive poloidal modes m and $m \pm 1$ couple to form a TAE gap. Recently, Zhixuan *et al* [34] reported interesting results on the radial localization of TAEs. The local value of the safety factor at which $m-1$ and m poloidal harmonics couple is $q\,(r_{m-1,\,m}) = (m-1\,/\,2)\,/n$, where $r_{m-1,\,m}$ is the radial location of mode rational surface. Similarly in the radially outward direction on the next mode rational surface, $r_{m,\,m+1}$ where the m and $m+1$ poloidal harmonics couple, the safety factor is $q\,(r_{m,\,m+1}) = (m+1\,/\,2)\,/n$. To excite the dual TAEs, we considered $\kappa_{nf}(r)$ profile having local maxima at radial positions $r_{m-1,\,m}$ and $r_{m,\,m+1}$.

To focus on the simultaneous excitation of TAEs for a single n, we have used a mock-up analytical profile using κ_{nf} as a control parameter. The four different cases as shown in figure 4 are considered to see the effect of the ratio of κ_{nf} at two neighboring mode rational surfaces.

5. Results and discussions

In the simulation we have considered non-monotonic fast particle density profiles, using the density gradients at two mode rational surfaces as control parameters i.e. $\kappa_{nf}(r_{5,6})$ and $\kappa_{nf}(r_{6,7})$. The excitation criteria and characteristic of TAEs are investigated. For the KSTAR type equilibrium used in this work, we have focused on the TAEs excited in the first two TAE gaps located at $r_{5,6} \equiv r/a \approx 0.42$ and $r_{6,7} \equiv r/a \approx 0.58$, radially apart at a distance of $\Delta r/a \approx 0.16$. At these radial locations, poloidal harmonics $m = 5$ couple with $m = 6$ and $m = 6$ couple with $m = 7$ to form two TAE gaps. It is found that to excite the multiple TAEs, $\kappa_{nf}(r_{6,7})$ must be much higher than the $\kappa_{nf}(r_{5,6})$, required to excite a localized TAE, which is not intuitively obvious.

Results for the case-I and case-II are shown in figure 6 in column wise, figure 7 shows results for case-III and case-IV, whereas the effect of the monotonic density profile is presented in figure 5 for comparison. In all of the figures 5–7, the first row of the figure shows the poloidal cross-section (for the normalized scalar potential Φ (left) and the normalized parallel vector potential $A_{\parallel}$ (right)), the second row shows the radial structure of the poloidal mode amplitude (for both Φ (left) and $A_{\parallel}$(right)), and the third row displays the frequency spectrum in the radial direction, which is overplotted on the ideal MHD Alfven continuum to illustrate the radial location and the frequency range for comparison. The frequency axis is normalized by the Alfven frequency at the axis i.e. $f_{A0} = v_A/(2\pi R) \approx 745$ KHz, which gives a center value of the TAE gap frequency $f_{TAE} \approx 153$ KHz.

Figure 5 shows the results for the case of monotonic density profile with a single density gradient peak $\kappa_{nf}(r_{5,6}) = 4.6$. A single localized TAE appears due to the coupling of $m = 5$ and $m = 6$ at the center of the first TAE gap. In figures 5(*a*) and (*c*), the poloidal mode structure of Φ ($A_{\parallel}$) shows a ballooning (antiballooning) behavior which is a typical characteristic of an even type TAE mode. Two poloidal harmonics $m = 5$ and 6 have dominant amplitude at the mode location, as shown in figures 5(*b*) and (*d*). Figure 5(*e*) shows the frequency spectrum and the radial location of a localized TAE with a dominant frequency at the first gap and relatively smaller radial extent.

For case-I and case-II, the radial profiles of $\kappa_{nf}(r)$ shown in figure 4 have $\kappa_{nf}(r_{5,6}) = 9.9$ and 4.6, respectively. For both cases $\kappa_{nf}(r_{6,7}) = 16.8$. Gyrokinetic simulation results for both cases are shown in figure 6 (in the left and right panels). In figures 6(*a*) and (*c*), the poloidal mode structure of Φ ($A_{\parallel}$) shows a ballooning (antiballooning) behavior. Two poloidal modes with $m = 5$ and 6 are the dominant modes with a small finite amplitude $m = 7$ mode, as shown in figures 6(*b*) and (*d*) for case-I. A relatively stronger $m = 7$ mode is shown in case-II (figures 6(*g*) and (*i*)). Because of this small finite amplitude, $m = 7$ poloidal harmonic, the mode structure slightly shifts towards right from the center of the first TAE gap, as shown in figures 6(*e*) (for case-I) and (*j*) (for case-II). Moreover for case-II, figure 6(*j*) also shows that the modes spread toward the neighboring TAE gaps. The simulation results show that even though the fast particle density gradient at the second gap is stronger than in the first TAE gap, i.e. $\kappa_{nf}(r_{6,7})/\kappa_{nf}(r_{5,6}) \approx 3.65$, but it is still not sufficient to excite two TAEs simultaneously.

Next, keeping $\kappa_{nf}(r_{6,7})$ fixed at $\kappa_{nf}(r_{6,7}) = 25.2$ and $\kappa_{nf}(r_{5,6})$ is changed slightly in two steps i.e. $\kappa_{nf}(r_{5,6}) = 4.6$ (case-III) and $\kappa_{nf}(r_{5,6}) = 3.1$ (case-IV). Simulation results for case-III (case-IV) are presented in figure 7 in the left (right) panel. The poloidal mode structure of Φ and $A_{\parallel}$ shows a break of radial symmetry due to the excitation of the two localized TAEs at two consecutive gaps of the Alfven continuum. The radial mode structure for Φ (figures 7(*b*) and (*g*)) shows three symmetric poloidal modes $m = 5$, 6 and 7 with the same polarities and significant mode amplitudes. It can be seen in the figures that the radial width of $m = 6$ mode is extended far to couple with both of its neighboring poloidal modes. Figures 7(*d*) (case-III) and (*i*) (case-IV) show the radial mode structures for the vector potential $A_{\parallel}$. For $A_{\parallel}$, the $m = 6$ mode becomes strongly anti-symmetric, and thus it couples to both the $m = 5$ and $m = 7$ modes simultaneously, which have opposite polarities to $m = 6$ mode near the first and second gaps, respectively. For case-III frequency spectrum in figure 7(*e*) shows that two discrete TAEs are excited and the mode strength in the first

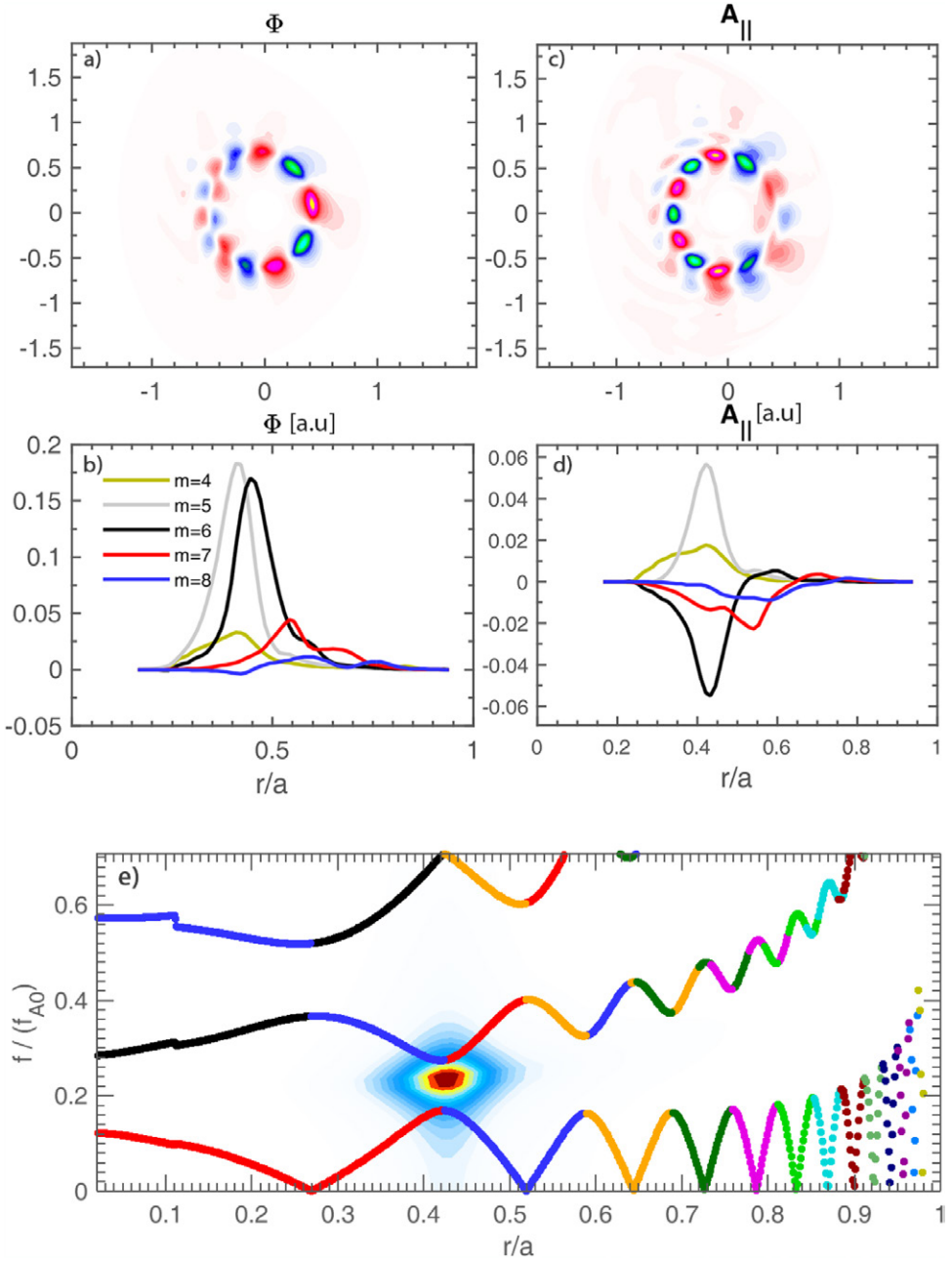

Figure 5. Poloidal mode structures and frequency spectra of a localized single TAE, for the case of the monotonically decreasing density profile.

gap is stronger than the one in the second gap for case-III. Whereas in case-IV the $m = 7$ mode has a large magnitude and $m = 6$ mode move towards the second gap position of the Alfven continuum. Hence a stronger TAE in the second gap is excited compared to the first gap, as evident from frequency spectrum shown in figure 7(j).

From the discussions above, it is clear that not only the absolute values of $\kappa_{\rm nf}$, but also the ratio $\kappa_{\rm nf}(r_{6,7})/\kappa_{\rm nf}(r_{5,6})$, representing the relative strength between the two density gradients, is important for the excitation of the second TAE. It is observed that $\kappa_{\rm nf}(r_{5,6})$ is more sensitive than the $\kappa_{\rm nf}(r_{6,7})$ for the excitation of the TAEs. In the simulation, the frequency difference between the two TAEs is shown to be $\Delta f/f_{\rm A0} = f(r_{6,7})/f_{\rm A0} - f(r_{5,6})/f_{\rm A0} \simeq 0.0120$ i.e. 8.94 KHz, whereas in KSTAR experiment the frequency difference is 9.6 KHz. For the parameters chosen, our simulation results show the value of the frequency difference in agreement with the experimental value, which indicates the dual modes with a single n observed in the experiment might in fact be due to the two TAEs excited at two nearby locations.

The pitch dependance in velocity distribution only adds a small amount of extra drive to the universal pressure gradient drive [45]. Thus, the inclusion of anisotropic beam ion distribution may not alter the conclusion of the present analysis. Since Alfvenic activity can drive fast-ion transport [47, 48], once the wave is excited the profiles will be flattened and the dual mode may disappear by the change of the profile gradient. Further research is required to understand the effect of

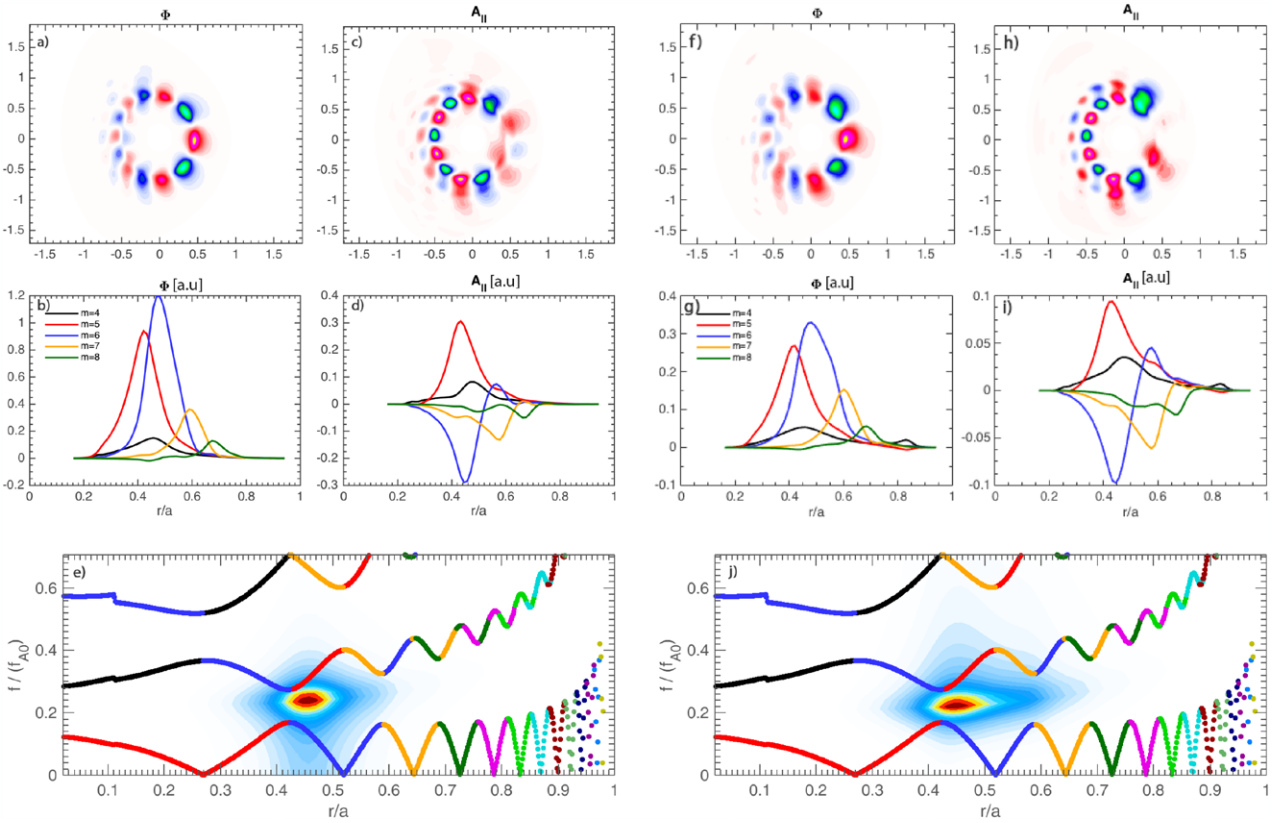

Figure 6. Poloidal mode structures and frequency spectra for case-I (left) and case-II (right).

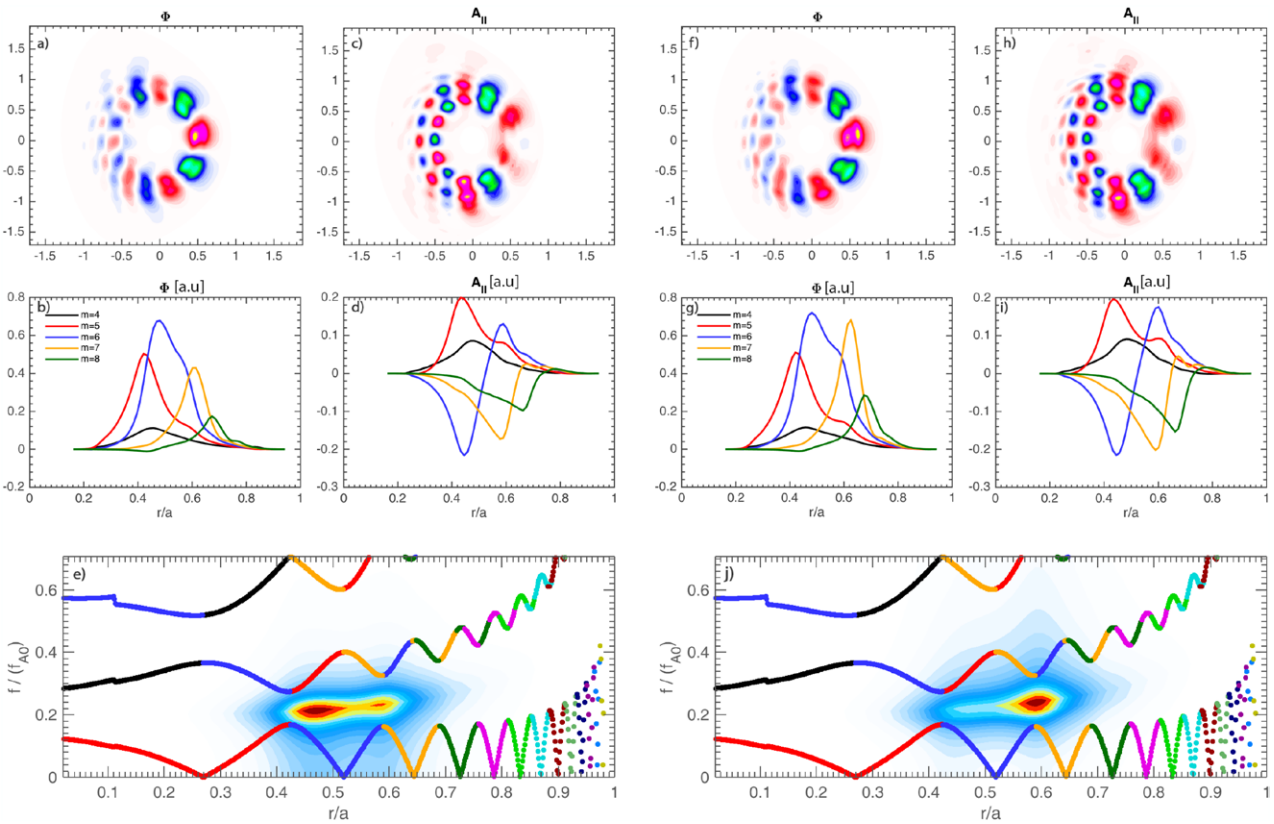

Figure 7. Poloidal mode structures and frequency spectra for case-III (left) and case-IV (right).

multiple TAEs on the fast ion transport, their local characteristics, and the effect on the profile flattening.

6. Conclusion

We report the observation of multiple TAEs found in KSTAR and the simulation study of these modes by using the GTC code. In the simulation, it is shown that the excitation of multiple TAEs depends on the critical shear and the relative strength between the fast ion density gradients at the positions where the modes are excited. If the conditions of the critical shear and the relative fast ion density gradients for the multiple modes are not satisfied, then the multiple TAEs do not seem to appear and rather a single global TAE mode is excited. Thus, excitation of two TAEs residing at different mode rational surfaces simultaneously is feasible, but exciting more than two TAEs looks difficult.

Acknowledgment

This work was supported by the grant from IBS (IBS-R012-D1-2015-a03) in Korea, and also by the National Research Foundation of Korea(NRF) No. NRF-2012K2A2A6000505 and No. NRF-2015M1A7A1A02050238.

References

[1] Pinches S.D. *et al* 2004 *Plasma Phys. Control. Fusion* **46** B187
[2] Zonca F. *et al* 2006 *Plasma Phys. Control. Fusion* **48** B15
[3] Heidbrink W.W. 2008 *Phys. Plasmas* **15** 055501
[4] Sharapov S.E. *et al* 2013 *Nucl. Fusion* **53** 104022
[5] Kramer G.J. *et al* 2004 *Phys. Rev. Lett.* **92** 015001
[6] Fredrickson E.D. *et al* 2006 *Nucl. Fusion* **46** s926
[7] Van Zeeland M.A. *et al* 2006 *Nucl. Fusion* **46** S880 135001
[8] Lauber Ph. *et al* 2012 *Nucl. Fusion* **52** 094007
[9] Gassner T. *et al* 2012 *Phys. Plasmas* **19** 32115
[10] Fasoli A. *et al* 2007 *Nucl. Fusion* **47** S264
[11] da Grac S. *et al* 2012 *Plasma Phys. Control. Fusion* **54** 095014
[12] Fasoli A. *et al* 1998 *Phys. Rev. Lett.* **81** 5564
[13] Vlad G. *et al* 2009 *Nucl. Fusion* **49** 075024
[14] White R. *et al* 2010 *Plasma Phys. Control. Fusion* **52** 045012
[15] Podesta M. *et al* 2012 *Nucl. Fusion* **52** 094001
[16] Schneller M. *et al* 2013 *Nucl. Fusion* **53** 123003
[17] Pinches S.D. *et al* 2015 *Phys. Plasmas* **22** 021807
[18] Schneller M. *et al* 2015 *Plasma Phys. Control. Fusion* **58** 014019
[19] Garcia-Munoz M. *et al* 2010 *Phys. Rev. Lett.* **104** 185002
[20] Van Zeeland M.A. *et al* 2006 *Phys. Rev. Lett.* **97** 135001
[21] Podesta M. *et al* 2011 *Nucl. Fusion* **51** 063035
[22] Melnikov A.V. *et al* 2010 *Nucl. Fusion* **50** 084023
[23] Kwak J.G. *et al* 2013 *Nucl. Fusion* **53** 104005
[24] Lin Z. *et al* 1998 *Science* **281** 1835
[25] Holod I. and Lin Z. *Phys. Plasmas* 20 032309
[26] Holod I. *et al* 2009 *Phys. Plasmas* **16** 122307
[27] Mishchenko A.M. *et al* 2011 *Phys. Plasmas* **18** 012504
[28] Tobias B.J. *et al* 2011 *Phys. Rev. Lett.* **106** 075003
[29] Todo Y. *et al* 2013 *Nucl. Fusion* **52** 094018
[30] Heidbrink W.W. 2013 *Nucl. Fusion* **53** 093006
[31] Todo Y. *et al* 2015 *Nucl. Fusion* **55** 073020
[32] Zhang W. *et al* 2012 *Phys. Plasmas* **19** 022507
[33] Zhang C. *et al* 2013 *Phys. Plasmas* **20** 052501
[34] Wang Z. *et al* 2013 *Phys. Rev. Lett.* **111** 145003
[35] Liu D. *et al* 2015 *Phys. Plasmas* **22** 042509
[36] Mandrekas J. 1992 Physics models and user's guide for the neutral beam module of the super-code, GTFR-102 *Technical Report* Georgia Institute of Technology, Atlanta, USA
[37] Rome J.A. *et al* 1974 *Nucl. Fusion* **14** 141
[38] Jinfang W. *et al* 2010 *Plasma Sci. Technol.* **12** 291
[39] Brizard A.J. and Hahm T.S. 2007 *Rev. Mod. Phys.* **79** 421
[40] Deng W. *et al* 2012 *Nucl. Fusion* **52** 023005
[41] Candy R. *et al* 1996 *Phys. Lett.* A **215** 299
[42] Turnbull A. *et al* 1993 *Phys. Plasmas* **7** 2546
[43] Luetjens H. *et al* 1996 *Comput. Phys. Commun.* **97** 219
[44] Xiao Y. *et al* 2015 *Phys. Plasmas* **22** 022516
[45] Wong H.V. and Berk H.L. 1999 *Phys. Lett.* A **251** 126
[46] Gorelenkov N.N. *et al* 2005 *Nucl. Fusion* **45** 226
[47] Heidbrink W.W. *et al* 2008 *Nucl. Fusion* **48** 084001
[48] Heidbrink W.W. *et al* 2007 *Phys. Rev. Lett.* **99** 245002